ISTITUTO NAZIONALE FISICA NUCLEARE

INFN/BE - 68/9
18 Luglio 1968

THE (π^-, nn) REACTION AT REST ON ^6Li, ^9Be and ^{12}C NUCLEI

F. Calligaris, C. Cernigoi and I. Gabrielli
I.N.F.N. - Sottosezione di Trieste

F. Pellegrini
I.N.F.N. - Sezione di Padova

SERVIZIO RIPRODUZIONE DELLA
SOTTOSEZIONE DI TRIESTE DELL'I

THE (π^-, nn) REACTION AT REST ON ^{6}Li, ^{9}Be and ^{12}C NUCLEI

F. Calligaris, C. Cernigoi and I. Gabrielli

Istituto Nazionale Fisica Nucleare - Sottosezione di Trieste

F. Pellegrini

Istituto Nazionale Fisica Nucleare - Sezione di Padova

18 Luglio 1968

A B S T R A C T

The absorption of negative pions at rest in ^{6}Li, ^{9}Be and ^{12}C nuclei has been investigated by the study of energy spectra and the momentum distributions of two neutrons, emitted at a correlation angle around 180 degrees. A time-of-flight technique has been used for the determination of the energy and the momentum of the neutrons.

* * *

1. - INTRODUCTION

There is theoretical evidence ([1]) that some information on nuclear structure and on nucleon pair correlations can be obtained by the study of reactions in which a pion is absorbed by a nucleus with a consequent emission of two or more energetic nucleons. In fact, if one assumes that the interaction is direct and that it does not involve the whole nucleus, then the simultaneous requirements of energy and momentum conservation lead to the conclusion that a two-nucleon absorption process is dominant as compared to a single nucleon interaction.

The study of the summed energy spectra of the emitted nucleons gives information on the two-hole excitations of the nucleus; in addition their relative momentum distribution, after the emission, is related to the momentum state and to the correlation of the nucleon pair in the nucleus before the absorption process. We performed this work limiting our attention to some nuclei involving the 1p shell, as is the case of ^{6}Li, ^{9}Be and ^{12}C. A time-of-flight technique has been used for the determination of the energies and the momenta of two neutrons emitted at a correlation angle around 180 degrees.

2. - EXPERIMENTAL TECHNIQUE

The experimental apparatus is shown in Fig. 1 and Fig. 2 and is similar to the reported in ref.([2])*), apart from the fact that a proton range telescope was inserted in order to investigate simultaneously (π^-,nn) and (π^-, np) reactions on the same nucleus; the results on the (π^-,np) reactions will be published in a following paper.

---

*) In that arrangement the distance of both neutron counters, with respect to the target, was 2.40 meters; also the angular acceptance was larger as compared to the present one. Because of these facts, the energy resolution and the angular uncertanity were poorer. The effect resulted in a broadening of the peaks in the summed energy spectra.

A beam of 120 MeV negative pions from the CERN Synchrocyclotron was brought to rest in targets of about 0.3 gr/cm^2 in thickness; this was possible because of the excellent energy definition of the beam realized at CERN. The thickness of the targets was so small in order to reduce at a minimum the energy losses of the outgoing charged particles in the (π^-,np) part of the experiment: a stopping rate of about 6.10^3 pions/sec was achieved in a 10×10 cm^2 area. Following a capture of a pion, a (π^-,nn) event was recognized by the detection of a neutron in the smaller scintillation counter in coincidence with another neutron detected in any of the three larger scintillation counters at the opposite side with respect to the target. The start signal of the time-of-flight of the neutrons was given by the output signal from the photomultiplier connected to the scintillation counter number 3 in Fig. 1 which was placed as close as possible to the target. This counter was a plastic scintillator of only 0.5 mm in thickness in order to minimize the absorptions of pions in the counter itself and also to minimize the energy losses of the outgoing charged particles in the (π^-, np) part of the experiment. The neutron detectors were plastic scintillation counters of 5 cm in thickness; the smaller one was a cylinder, 40 cm in diameter, viewed at the rear by a 58 AVP photomultiplier while the other one was a system of three scintillation counters, 45×135 cm^2 in area. This system was build in such a way to approximate a spherical surface in order to minimize the differences in path from the target to the detectors. Each of these counters was viewed, at the opposite shorter sides, by two 58 AVP phomultipliers. Due to the large lenght of these counters, the true time-of-flight of a neutron, hitting them, was measured by taking the mean value of the apparent times-of-flight determined separately by each photomultiplier.

On the other hand, this arrangement enabled us to measure, the relative angles of emission (to a certain extent) of the emitted neutrons, by taking the difference of the above mentioned times-of-flight. A relative time calibration of the system was done by means of light signals of simultaneously triggered hydrogen discharge lamps; an absolute calibration was then given by the position of the peak corresponding to the ground state of ^{4}He in the reaction:

$$\pi^- + {}^6\mathrm{Li} \rightarrow {}^4\mathrm{He} + 2n$$

The counter number 4 in Fig. 1 acted as an anticoincidence in the beam telescope to detect a stopped pion and also as an anticoincidence for the larger neutron detector system.

The electronic logic is shown schematically in Fig. 3; its main features are the following: identification of (π^-,nn) events with localization in the larger neutron detector system, selection of the pulses generating these events from the photomultipliers and, finally, time-to-height conversion of these pulses *). After this procedure a suitable counting and memory system was used to take the relevant data of the events, namely number of stopped pions and three separate times-of-flight; the data were recorded on a tape for further analysis.

The proton range telescope acted as an anticoincidence counter for the smaller neutron detector in the present experiment. The overall time resolution of the system is of the order of 1 nsec which, with the distances of the neutron counters, was quite sufficient to separate clearly two peaks in the summed energy spectrum of ^{6}Li (see later in the text). The energy resolution is increasing in the higher excitation region corresponding to the lower part of the summed energy spectrum.

---

*) From the electronic logic it was also possible to recognize (π^-,nn) events when one neutron was converted in the proton range telescope; these events were counted but any time analysis was not possible for them. The proton range telescope consisted of a "sandwich" of 30 plastic scintillators, each of them connected to a photomultiplier. Any charged particle, traversing the telescope or some part of it, was identified by the signals of the photomultipliers connected to the respective plastic scintillators.

3. - ENERGY SPECTRA

The summed energy spectra for ^{6}Li, ^{9}Be and ^{12}C are displayed in Fig.4 *), where on the ordinate the number of neutron pairs per MeV per stopped pion per sterad^2 is reported. This number has been calculated according to an evaluation of about 3.10^{-3} for the combined efficiency of the two neutron counters. This evaluation may lead to an error of about 40% in the absolute absorption rate for the process under investigation because of the uncertainties in the efficiency of plastic scintillators. On the abscissa the sum of the energies of the detected neutrons is reported.

All these spectra present pronounced peaks near the threshold of the corresponding reactions; only the ^{6}Li spectrum presents a more complex structure. In order to derive the excitation spectrum of the residual nucleon system, an evaluation of the momentum sum $\vec{K} = \vec{k}_1 + \vec{k}_2$ (see Fig. 2) of the two neutrons was first done, according to a procedure discussed later in the paper. After this, the energy recoil of the residual nucleon system in each case has been evaluated and the excitation energy spectra for the three nuclei correspondingly derived.

3.1 - ^{6}Li (π^-, nn) ^{4}He reaction.

In Figs. 5 and 6 the excitation energy spectra for the ^{6}Li case are displayed. In Fig. 5 the excitation spectrum is reported for three different ranges of the recoil momentum $|\vec{K}| = |\vec{k}_1 + \vec{k}_2|$ and for a neutron threshold energy of about 20 MeV; in Fig. 6 the same spectra are reported for a neutron threshold energy of 35 MeV. The first threshold has been experimentally determined by our time-of-flight acceptance interval while the second one has been introduced in the data analysis in order to see the influence of a higher neutron threshold on our energy spectra. By inspection of Figs. 5a, 5b and 5c one can see that the first peak, corresponding to the transition leading to the ^{4}He ground state is composed mainly by events of less than 100 MeV/c of recoil momentum. On the other hand, the second peak (at an excita-

*) All the curves in the following figures of this paper are only tentative fits of the experimental points.

tion energy of about 30 MeV) seems to have a more complex structure as the range of momentum recoil is restricted to values lower than 100 MeV/c; there is some indication that this structure may consist of two peaks, occuring at 30 and 40 MeV, within our experimental resolution and statistics. It is to be remarked that our energy resolution in this part of the spectrum is almost double than in the first peak, simply because the neutron energies involved are much lower. Anyway it is clear that the peak at 30 MeV is strongly depressed when events of less than 100 MeV/c are considered; this fact is confirmed by comparison of Figs. 5b, 6a and 6b, which show that also the cut of events with less than 35 MeV for each neutron affects the height of this peak, without changing significantly the ^{4}He peak. The value of 35 MeV threshold has been chosen in connection with the different sensitivities of the two neutron counters in the energy region below 35 MeV; for the smaller counter there is an excess of low energy neutrons, as it can be seen from Figs. 7a and 7b. From a shell model point of view the possible absorbing nucleon pairs in ^{6}Li can be the $(p)^{-2}$, (ps) and $(s)^{-2}$ respectively; the corresponding peaks ahould be found at an energy excitation of 0, 20 and 30 MeV ([3]). There are several arguments (low correlation between p and s nucleons) which lead to the conclusion that the 20 MeV peak has a low probability to be excited. From our experimental results there is evidence of two peaks, one corresponding to the ground state of ^{4}He, already found in the experiment of ref. ([4]), and the other one at 30 MeV in excitation. An eventual peak at 20 MeV does not appear clearly, within our energy resolution, although can not be excluded. In an alpha-deuteron cluster model of ^{6}Li one should expect mainly two peaks, one corresponding to the absorption on the peripheral deuteron, the other one corresponding to the absorption on the alpha structure with its consequent partial or total break-up; in the latter case, the corresponding peak should start at an excitation energy of about 22 MeV. These predictions were confirmed experimentally by the Authors of ref. ([5]), which results are in fairly good agreement with ours, although their experiment concerned $(\pi^{\pm},2p)$ interaction in flight.

3.2 - ^{9}Be(π^-,nn) ^{7}Li and ^{12}C(π^-,nn) ^{10}B reactions.

In Fig. 8 the excitation energy spectra of ^{9}Be and ^{12}C are displayed.

The spectrum restricted to events less than 100 MeV/c in recoil momentum is reported only for ^{9}Be because for ^{12}C the statistics is too poor; this is due partly to the fact that is was found experimentally that the relative absorption rate in this nucleus is 0.50 as compared to the ^{6}Li nucleus while in ^{9}Be is 0.80, if we normalize to 1 the absorption rate in ^{6}Li. From the figure one can see that the ^{9}Be and ^{12}C spectra are similar in shape, showing a peak near the zero excitation energy and a more or less smooth tail towards the higher energy excitation region. The main difference between the two spectra is the position of the peaks; in ^{9}Be the maximum of the spectrum occurs at about 10 MeV while in ^{12}C the maximum is nearer to the zero point. From the shell model point of view, this can be explained by the fact in the reaction on ^{9}Be the residual ^{7}Li nucleus presents only 5 known levels up to an excitation energy of 10 MeV which will contain a small fraction of the $(p)^{-2}$ configuration. On the other hand, in the reaction on ^{12}C, the residual ^{10}B nucleus presents more than 25 levels up to an energy excitation of 10 MeV which will probably exhaus all the $(p)^{-2}$ configuration. From Fig. 8b it can be seen that there is evidence that also s-nucleons take part in the absorption process in ^{9}Be.

In Figs. 9a and 9b the one neutron spectra, corresponding to (π^{-},nn) events, are reported. The main features of these spectra is the absence of any pronounced dip, within our statistical error. In connection with the paper of ref. ([6]), this fact may indicate that the observed (n,n) pairs come mainly from absorption in the 1S atomic orbit of the pions or, if there are contributions from the 2P orbit, the final state interaction does not play a so important role as claimed by these Authors.

We believe that much more experimental effort should be devoted to the study of these more complex nuclei to see to what extent this kind of process may play an important role in nuclear structure investigations.

4. - MOMENTUM DISTRIBUTIONS

As previously stated, it was possible to obtain experimentally, to a certain extent, the angle α between the two detected neutrons. This was ne

cessary in our experiment because one can see from Fig. 2 that in our geometrical conditions, it is not possible to approximate the angle α as 180 degrees; in fact the maximum angle of acceptance ϑ is of the order of 16 degrees. The procedure adopted is the following: from an approximate evaluation of the hitting point of a neutron on the larger detecting system, $\cos \vartheta$ is calculated according to the formula:

$$\cos \vartheta = \frac{D}{\sqrt{D^2 + X^2 + Y^2}}$$

where X and Y are the coordinates of the hitting point and D is the distance between the target and the counter (see Fig. 2). The coordinate X, along the larger dimension of each counter, was measured, within 15 cm, from the difference between the apparent times-of-flight previously mentioned. In the direction normal to this one, the uncertainty in the coordinate Y corresponds only to the lateral dimensions of each counter (45 cm), because the electronic indicated the counter involved in the event. Y is assumed equal to $(R \times 22.5)$ cm for the central detector and equal to $(R \times 45 + 22.5)$ cm for the other two detectors, R being a random number between 0. and 1.. *).

From Fig. 2 the recoil momentum K of the residual system of nucleons is given by the following formula:

---

*) This procedure is performed under the non restrictive hypothesis that the angular distribution is constant within our angular uncertainty. It has been verified that a different sequence of random numbers R, does not affect either the recoil momentum spectra or the excitation energy spectra. The extension of the random fluctuations of the quantity Y to the value $(R \times 42.5)$ cm for the central detector and to $(2.5 + R \times 85.)$ cm for the other ones, in order to include the angular uncertainty of the smaller detector, leaves unchanged the excitation energy spectra and affects the recoil momentum spectra only within the actual statistical error. The angular distributions within our geometrical acceptance were not plotted; they are slowly monotonic decreasing functions of ϑ.

$$K = [(k_1 - k_2)^2 + 2k_1 k_2 (1 - \cos \alpha)]^{1/2}$$

where k_1 and k_2 are the measured absolute values of the neutron momenta, $\vartheta = 180° - \alpha$. The distributions, as function of K, of the quantities so calculated, are displayed in Fig. 10a, 10b and 10c, for the three nuclei under investigation. On the ordinate, the quantity:

$$\frac{\partial W(k)}{\partial K} = \int_{-0.98}^{-1} \frac{\partial^2}{\partial K \, \partial y} \, dy$$

with $y = \cos \alpha$ is reported in arbitrary units. In the case of ^{6}Li two curves are plotted on the same diagram, corresponding to events belonging to the ^{4}He peak and the remaining ones respectively.

From a theoretical point of view (Ref.(^{7})), it is perhaps more interesting to know the quantity:

$$\left. \frac{\partial^2 W(k)}{\partial K \, \partial y} \right|_{y = -1}$$

which can be evaluated experimentally only under the condition of vanishing detector solid angle. This was approximately true in the experiment of reference (^{4}); in our case this approximation is very crude. On the other hand a selection of events around the center of our counter system has to poor statistic to be physically significant. Anyway the momentum distributions, obtained by assuming $\cos \alpha = -1$ (i.e. considering $K = k_1 - k_2$), are reported in Figs. 11a, 11b and 11c, for the three nuclei respectively. Looking at all these distributions, it is to be noted the progressive broadening of the curves, going from ^{6}Li to ^{12}C, a fact which can be certainly attributed to the different momentum states of the nucleon pair before the absorption process. (Ref. (^{8}) and (^{9})).

* * *

ACKNOWLEDGEMENTS

We are indebted to the CERN machine staff for the continuous aid during the experiment; in addition we are grateful to R. Meunier, M. Spighel and J.P. Stroot for their information about the 120 MeV pion beam characteristics. We are also grateful to T.E.O. Ericson for his continuous interest in this experiment and to J. Sawicki, G. Alberi and L. Taffara for helpful discussions on the argument.

* * *

REFERENCES

(1) T.E.O. Ericson; Phys. Lett. 2, (1962), 278.

T.E.O. Ericson; Proceedings of the International Conference on High Energy Physics and Nuclear Structure, CERN Geneva 1963.

(2) F. Calligaris, C. Cernigoi and I. Gabrielli; π^- absorption in ^{6}Li and ^{12}C with two nucleon emission; Symposium on Light Nuclei, Brela - Yugoslavia, 1967, Gordon-Breach Inc.(In press).

(3) Y. Sakamoto; Nuclear Physics, 87, (1966), 414.

(4) H. Davies, H. Muirhead and J.N. Woulds; Nuclear Physic 78, (1966),663.

(5) G. Charpak, G. Gregoire, L. Massonet, J. Saudinos, J. Favier, M. Gusakow and M. Jean; Phys. Lett. 16, (1965), 54.

(6) G. Charpak, J. Favier, L. Massonet and C. Zupancic; Int. Conf. on Nuclear Physics, Gatlinburg - Tennessee, 12-17 Sept.1966.

C. Zupancic; Proc. Second Int. Conf. on High Energy Physics and Nuclear Structure, Rehovoth, 1967.

T. Bressani, G. Charpak, J. Favier, L. Massonet, W.E. Meyerhof and C. Zupancic; Phys. Lett. 25B, (1967), 409.

(7) J.M. Eisenberg and J. Letourneux; Nuclear Physics B3, (1967), 47.

(8) D.S. Koltun and A. Reitan; Phys. Rev. 155, (1967), 1139.

G. Alberi and L. Taffara: to be published in Nuovo Cimento.

(9) D.S. Koltun; Phys. Rev. 162, (1967), 963.

(10) F. Pellegrini; Nuovo Cimento, X, 54B, (1968), 335.

FIGURE CAPTIONS

Fig. 1 - Experimental set-up.

Fig. 2 - a) Geometrical acceptance and b) kinematical relation between the two neutron momenta.

Fig. 3 - Electronic block-diagram.

Fig. 4 - Summed energy spectra for ^{6}Li, ^{9}Be and ^{12}C.

Fig. 5 - Excitation energy spectra of ^{6}Li with 20 MeV neutron threshold; a) 0-230 MeV/c, b) 0-100 MeV/c and c) 100-230 MeV/c.

Fig. 6 - Excitation energy spectra of ^{6}Li with 35 MeV neutron threshold; a) 0-180 MeV/c, b) 0-100 MeV/c and c) 100-180 MeV/c.

Fig. 7 - ^{6}Li energy spectra of one neutron, correlated in a (π^{-},nn) event; a) smaller counter, b) counter system.

Fig. 8 - Excitation energy spectra of ^{9}Be and ^{12}C with 20 MeV neutron threshold; a) ^{9}Be, 0-230 MeV/c, b) ^{9}Be, 0-100 MeV/c and c) ^{12}C,0-230 MeV/c.

Fig. 9 - Energy spectra of one neutron, correlated in a (π^{-},nn) event; a) ^{9}Be target nucleus and b) ^{12}C target nucleus.

Fig. 10 - Recoil momentum spectra corresponding to the nuclei; a) ^{6}Li, b) ^{9}Be and c) ^{12}C.

Fig. 11 - Recoil momentum spectra, obtained by assuming $\cos \alpha = -1$, corresponding to the nuclei; a) ^{6}Li, b) ^{9}Be and c) ^{12}C.

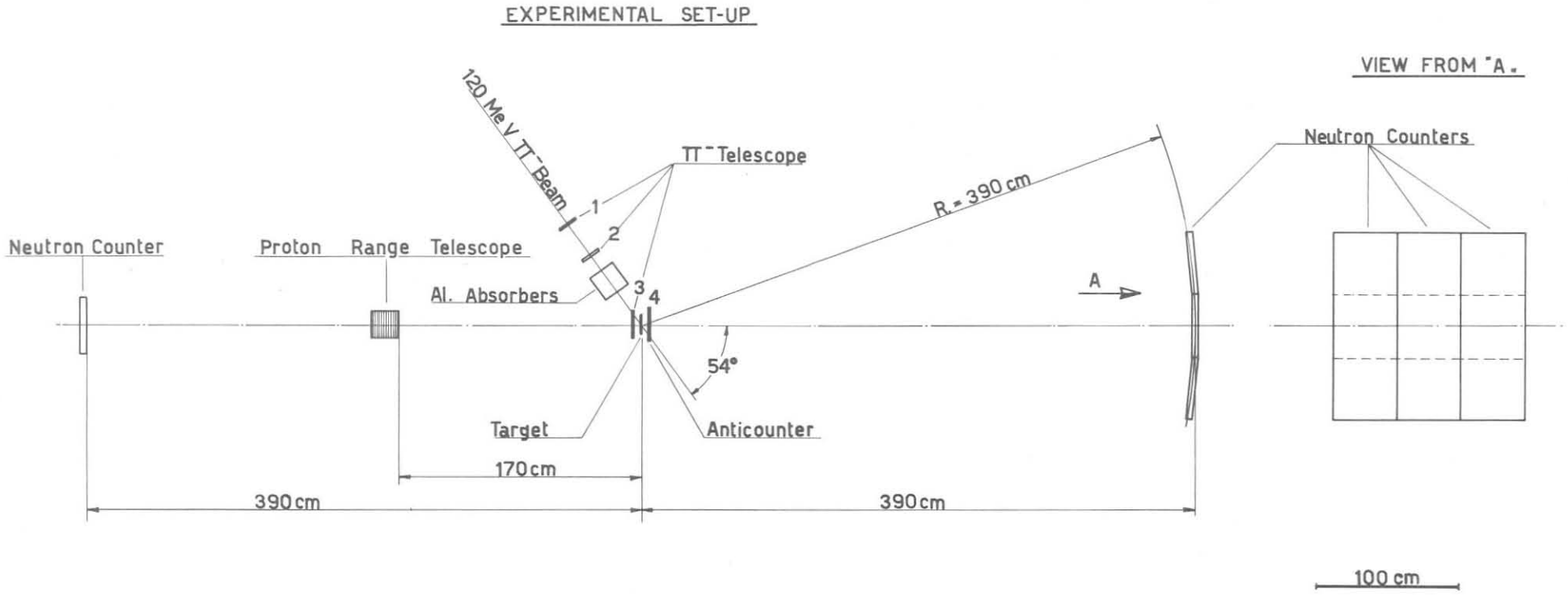
EXPERIMENTAL SET-UP
VIEW FROM "A"
120 MeV π⁻ Beam
1
2
π⁻ Telescope
R = 390 cm
Neutron Counters
Neutron Counter
Proton Range Telescope
Al. Absorbers
3
4
A
54°
Target
Anticounter
170 cm
390 cm
390 cm
100 cm

Fig. 1

1993

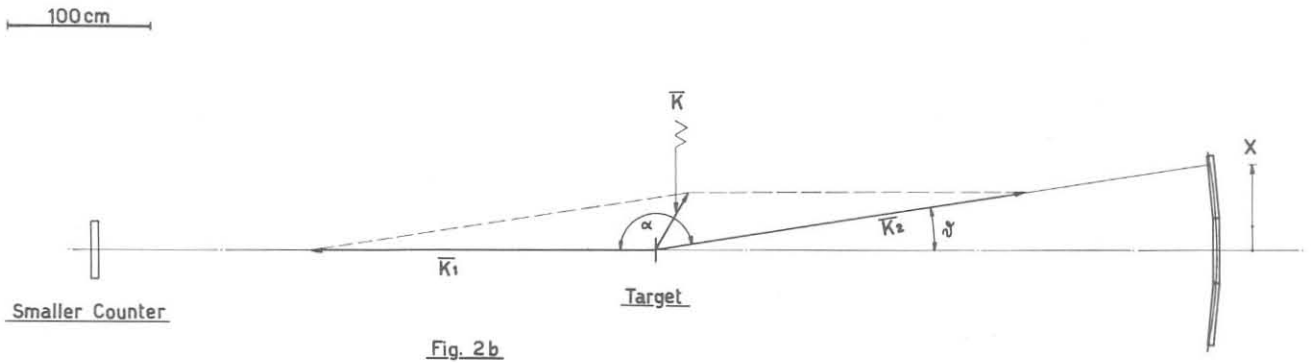

Fig. 2b

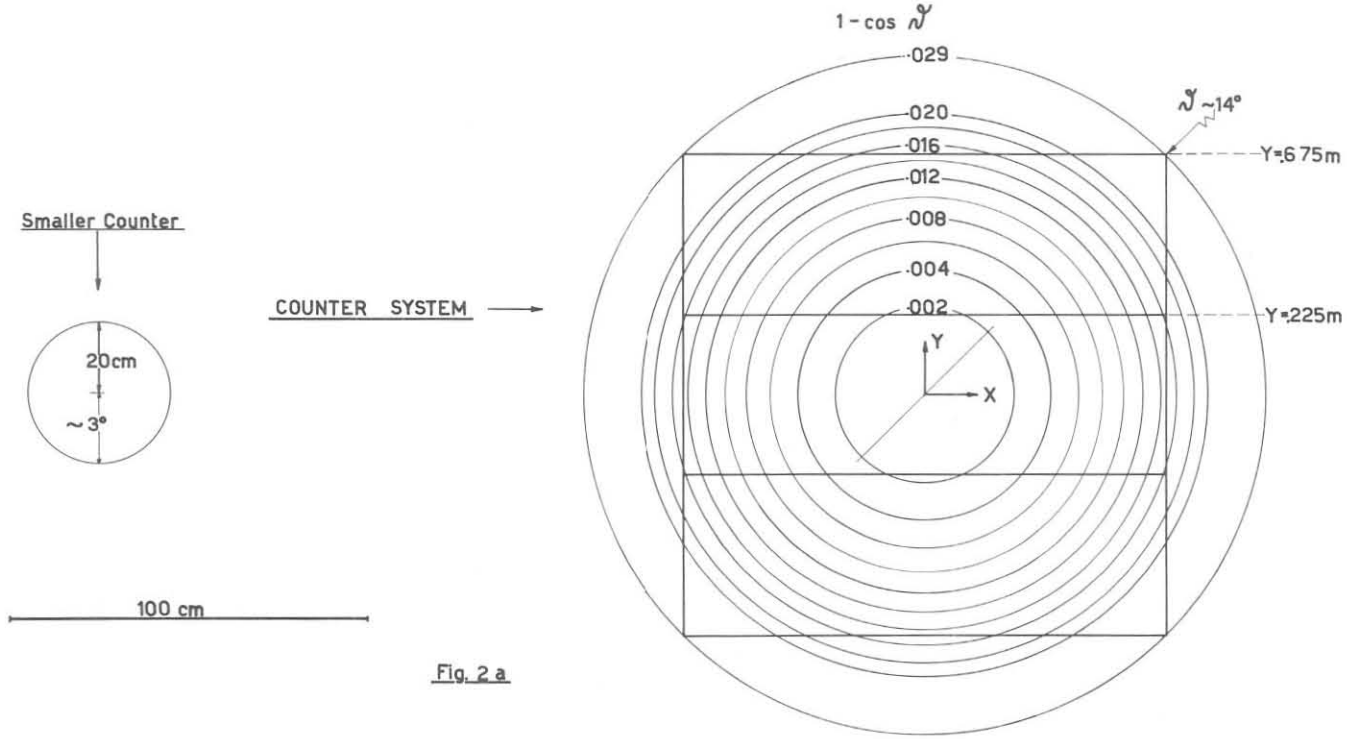

Fig. 2a

Fig. 2

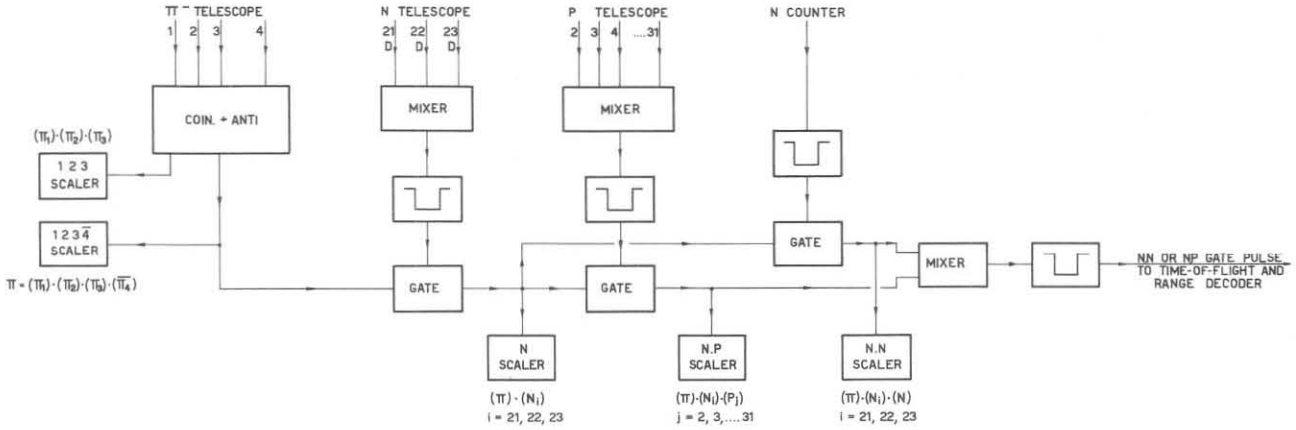
π⁻ TELESCOPE
1 2 3 4
N TELESCOPE
21 22 23
D D D
P TELESCOPE
2 3 4 31
N COUNTER
COIN. + ANTI
MIXER
MIXER
(π1)·(π2)·(π3)
1 2 3
SCALER
1 2 3 4̄
SCALER
π⁻ = (π1)·(π2)·(π3)·(π4̄)
GATE
GATE
GATE
MIXER
NN OR NP GATE PULSE
TO TIME-OF-FLIGHT AND
RANGE DECODER
N
SCALER
(π)·(Ni)
i = 21, 22, 23
N.P
SCALER
(π)·(Ni)·(Pj)
j = 2, 3,....31
N.N
SCALER
(π)·(Ni)·(N)
i = 21, 22, 23

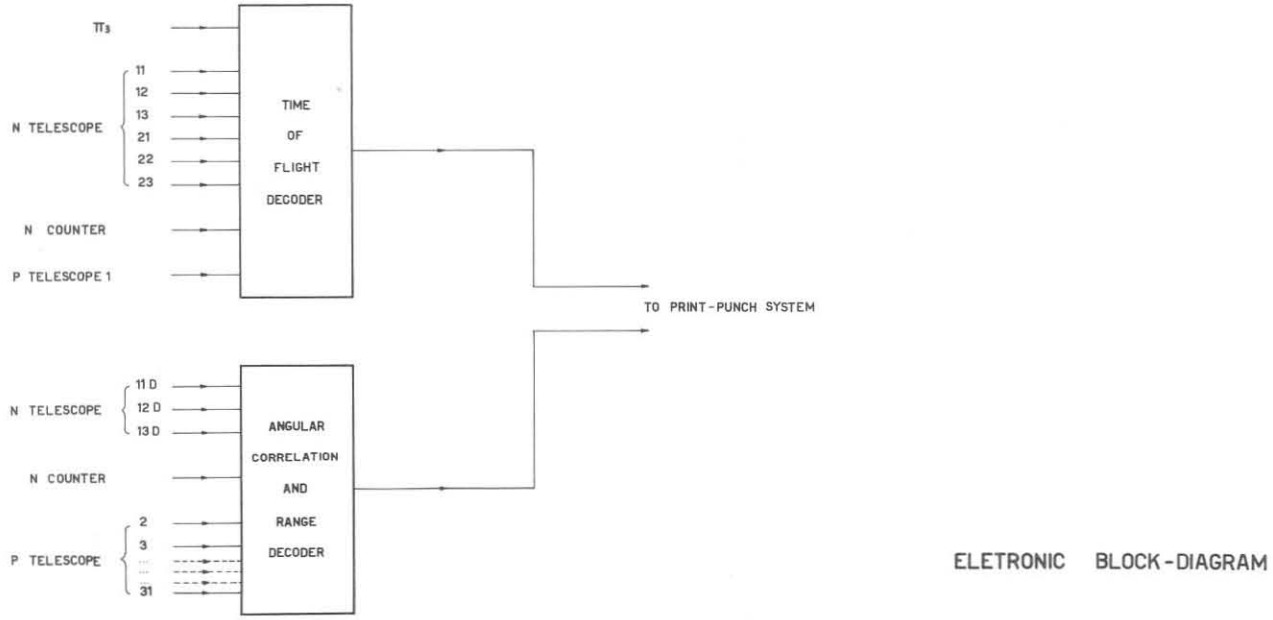
π3
11
12
13
21
22
23
N TELESCOPE
N COUNTER
P TELESCOPE 1
TIME
OF
FLIGHT
DECODER
TO PRINT-PUNCH SYSTEM
11 D
12 D
13 D
N TELESCOPE
N COUNTER
2
3
...
31
P TELESCOPE
ANGULAR
CORRELATION
AND
RANGE
DECODER
ELETRONIC BLOCK-DIAGRAM

Fig. 3

Fig.4

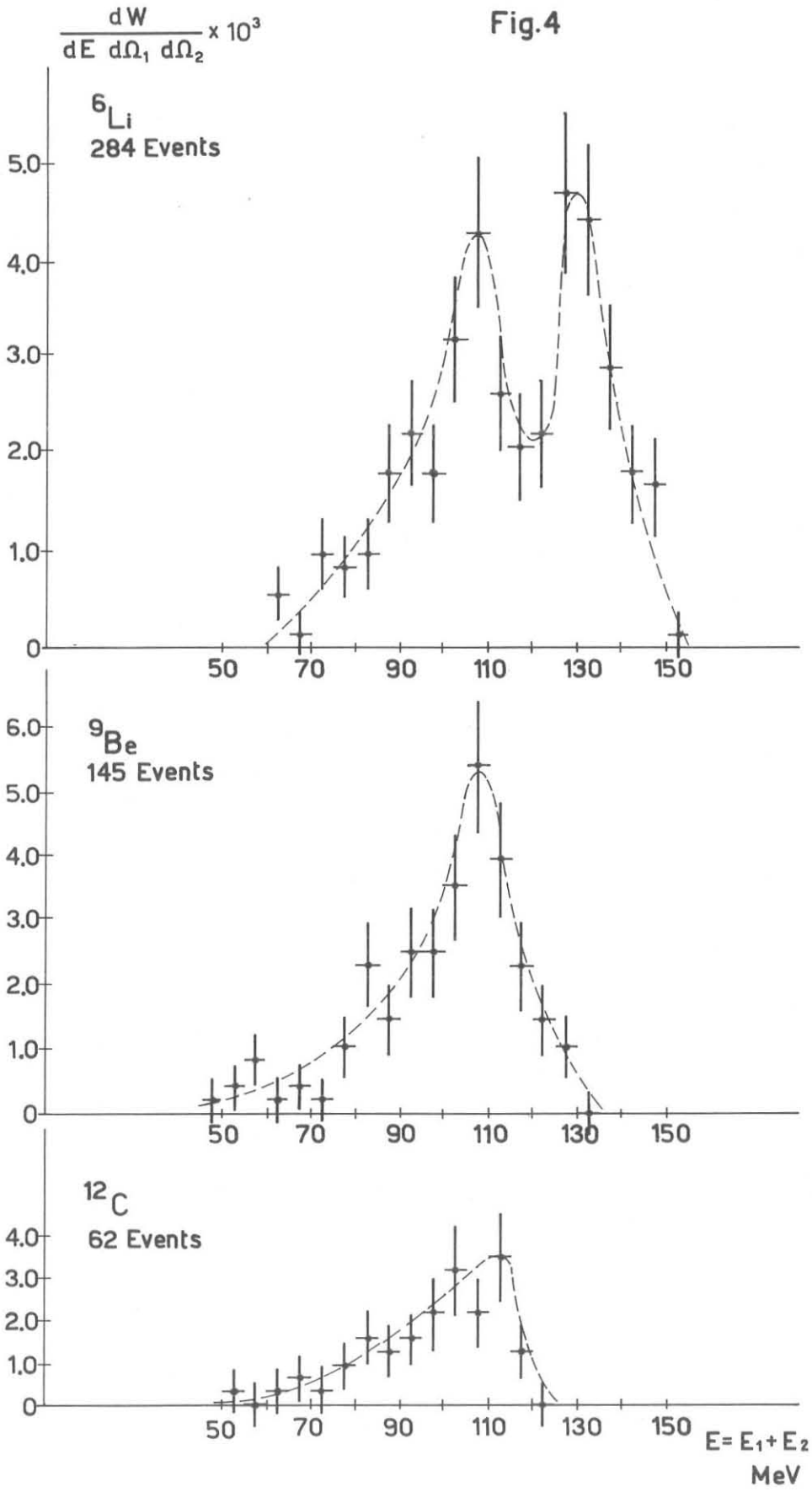
dW / dE dΩ1 dΩ2 x 10³
6Li
284 Events
9Be
145 Events
12C
62 Events
0
1.0
2.0
3.0
4.0
5.0
6.0
50
70
90
110
130
150
E= E1 + E2
MeV

Fig. 5

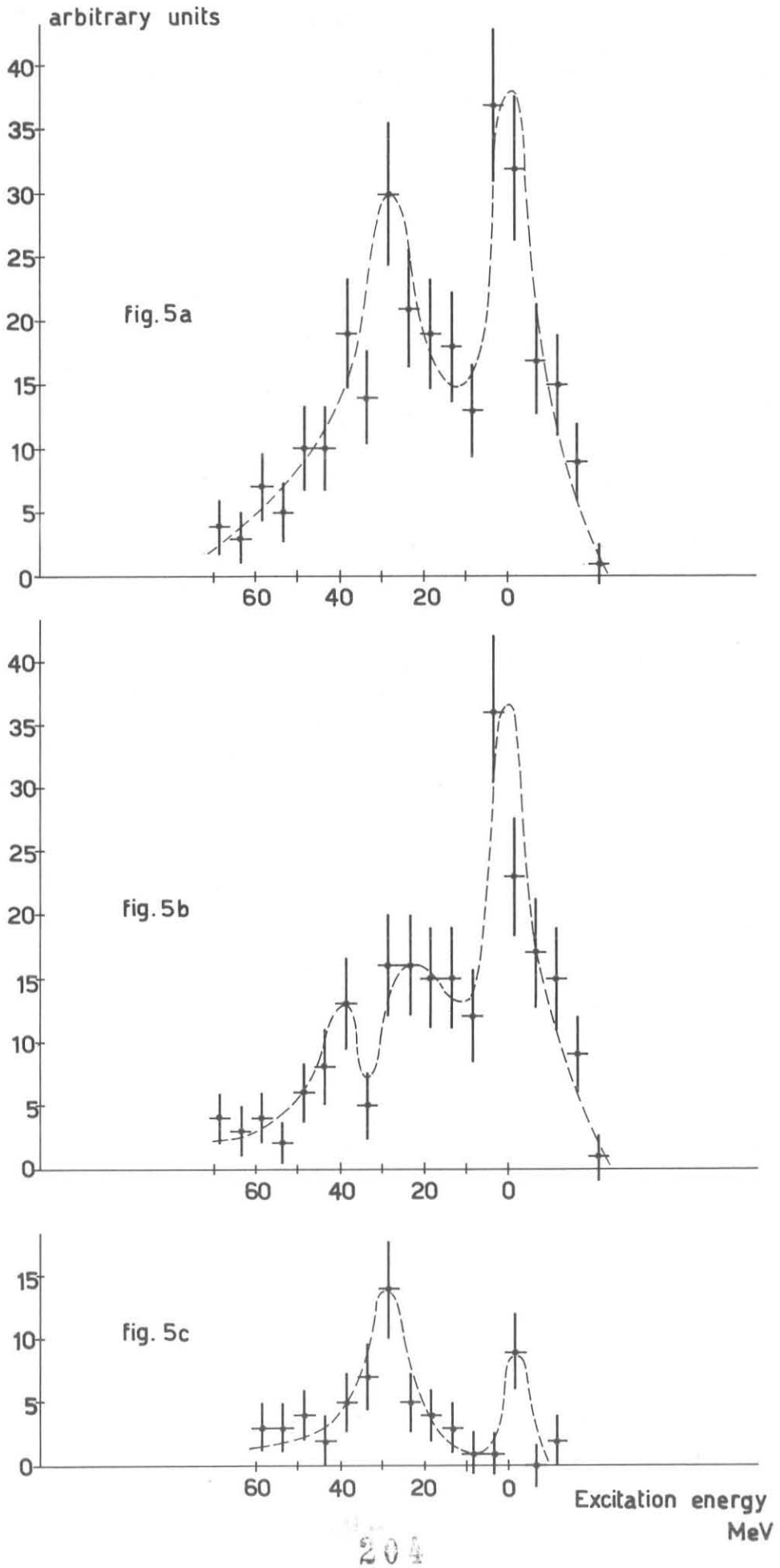

Fig. 6

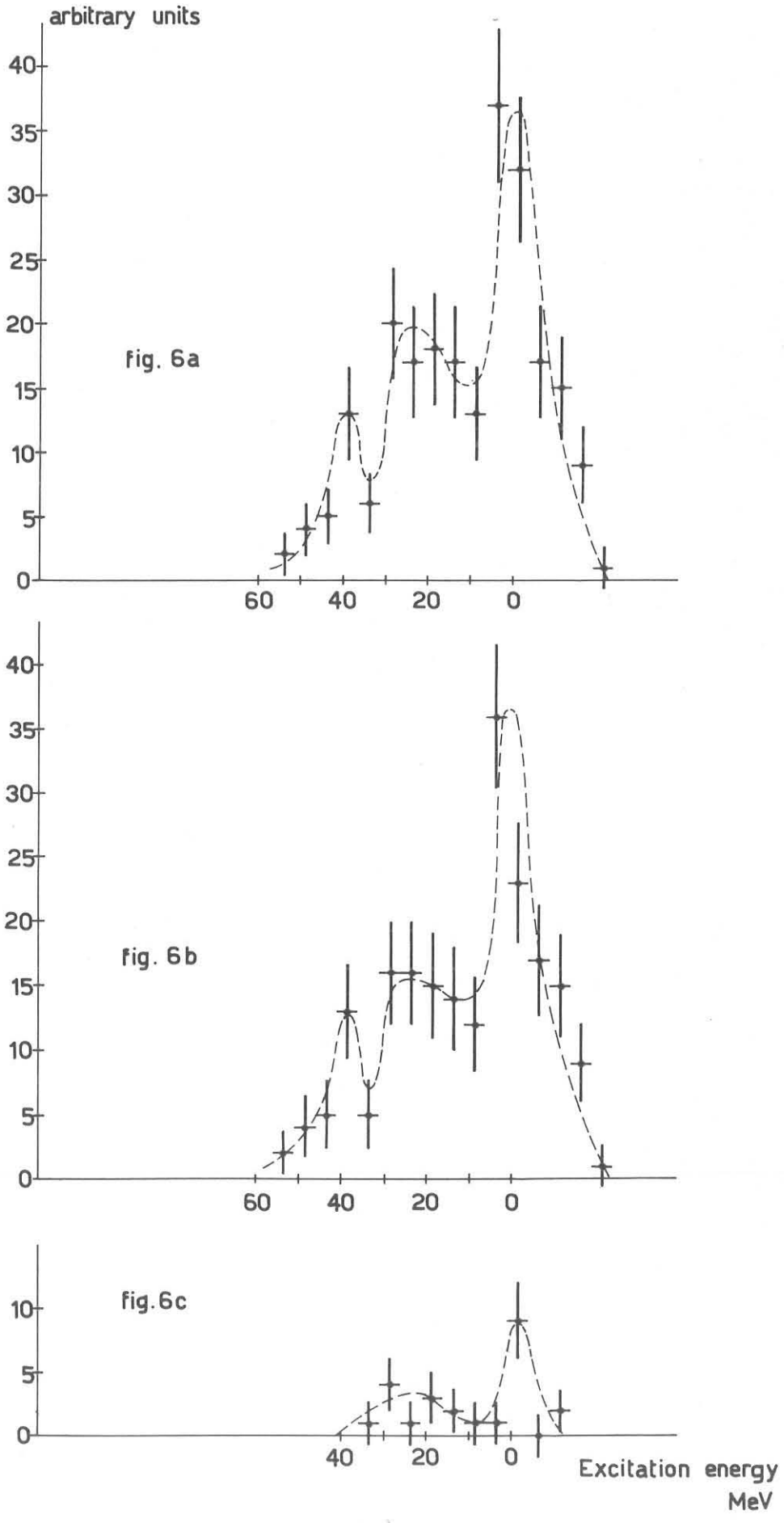
arbitrary units
40
35
30
25
20
15
10
5
0
fig. 6a
60
40
20
0
fig. 6b
fig. 6c
Excitation energy
MeV

Fig.7

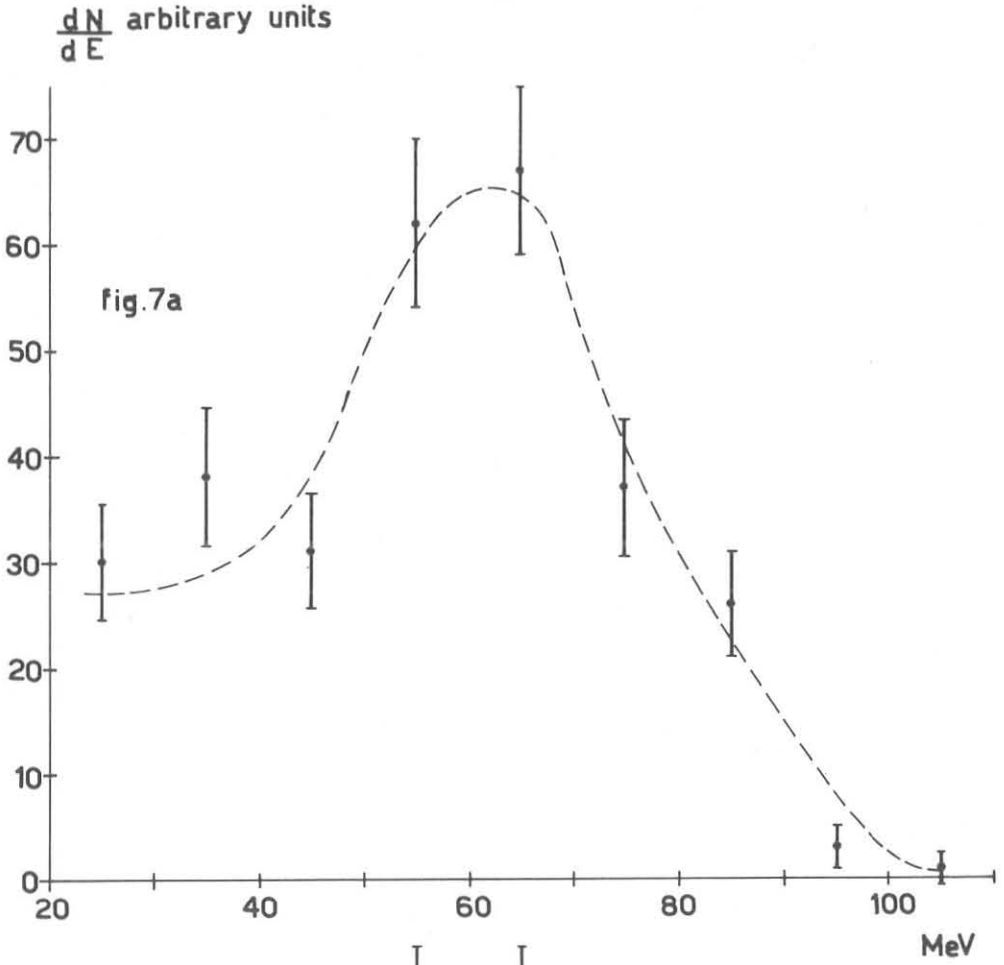
dN/dE arbitrary units
fig.7a
70
60
50
40
30
20
10
0
20
40
60
80
100
MeV

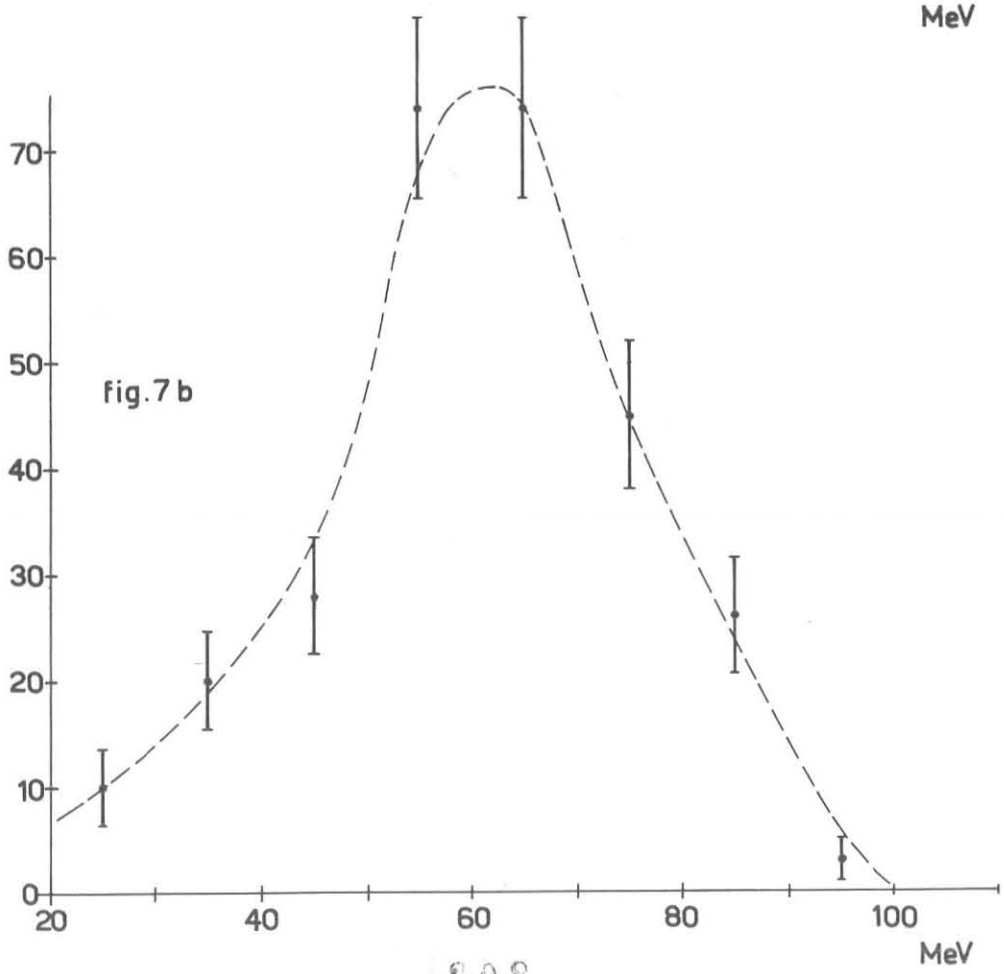
fig.7b
70
60
50
40
30
20
10
0
20
40
60
80
100
MeV

Fig. 8

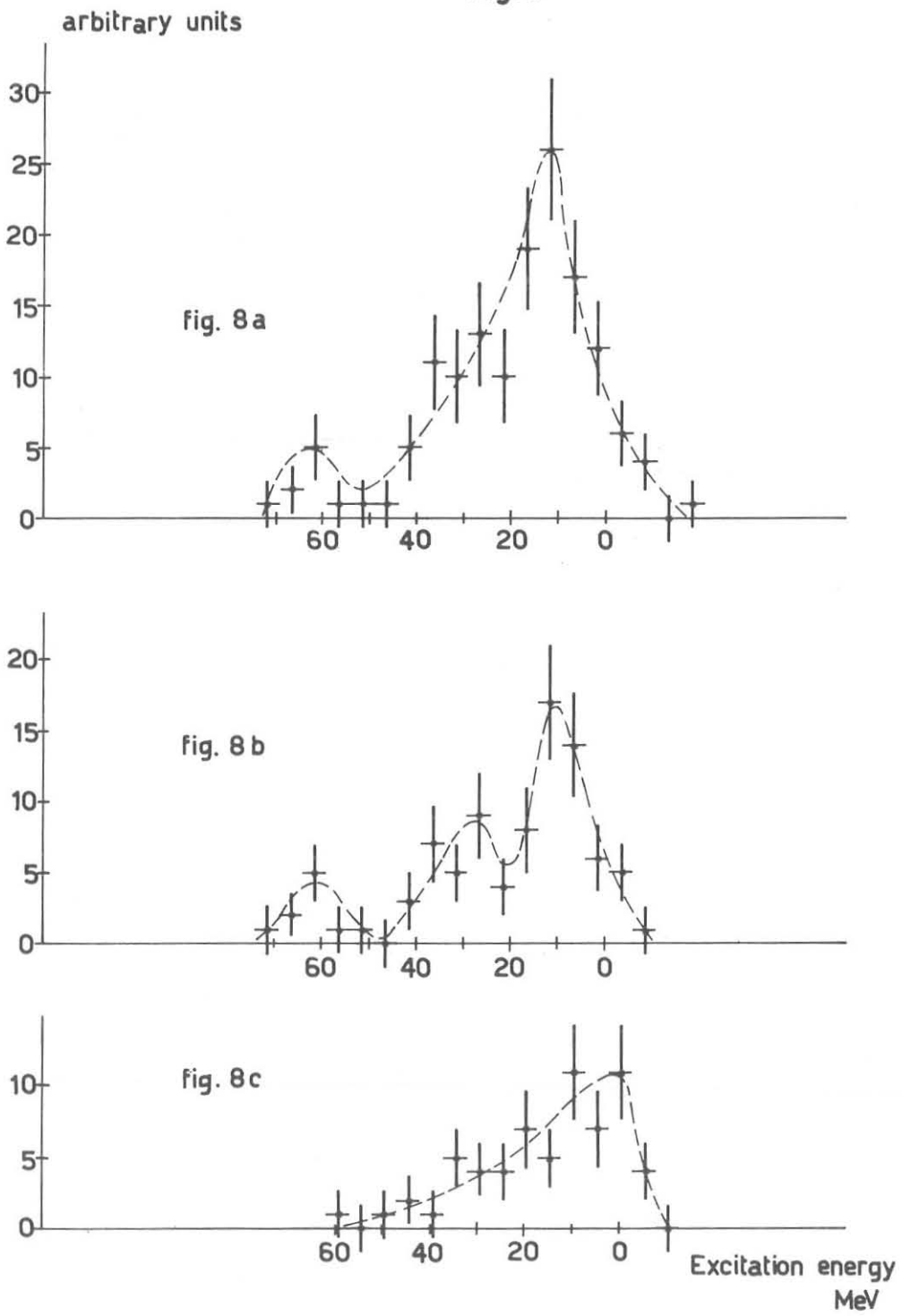
arbitrary units
30
25
20
15
10
5
0
fig. 8a
60
40
20
0
20
15
10
5
0
fig. 8b
60
40
20
0
10
5
0
fig. 8c
60
40
20
0
Excitation energy
MeV

Fig. 9

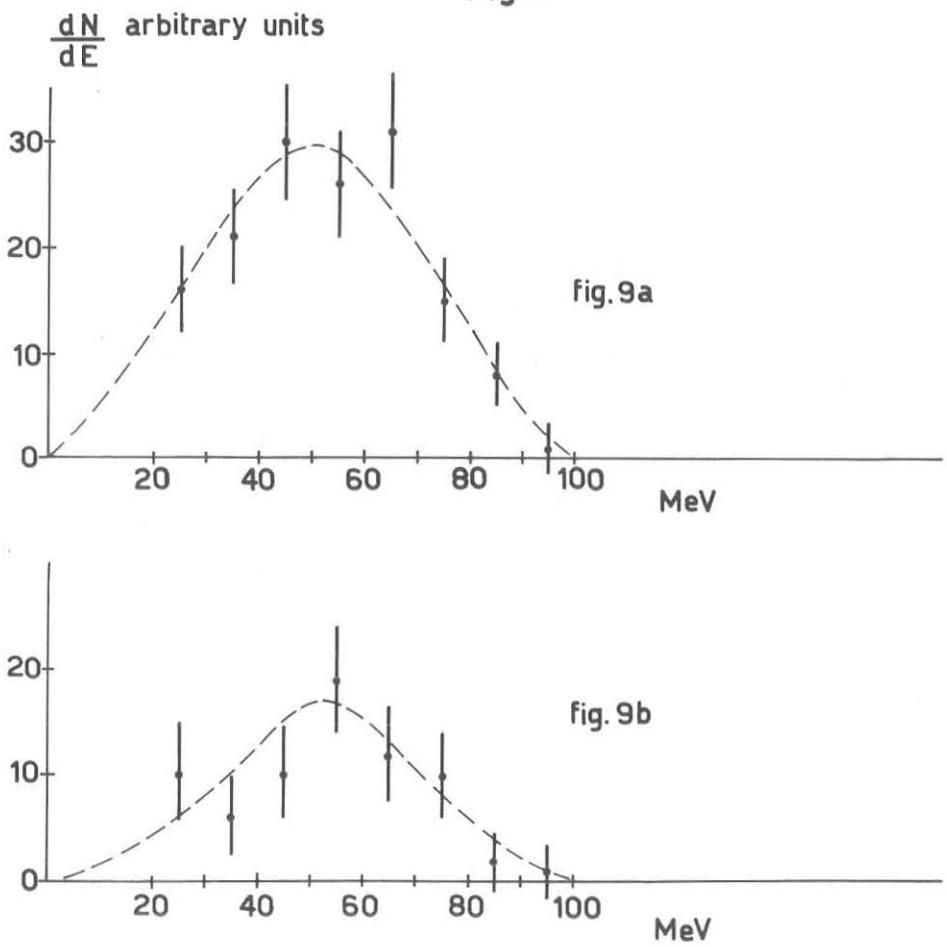
dN/dE arbitrary units
30
20
10
0
20
40
60
80
100
MeV
fig. 9a
20
10
0
20
40
60
80
100
MeV
fig. 9b

Fig.10

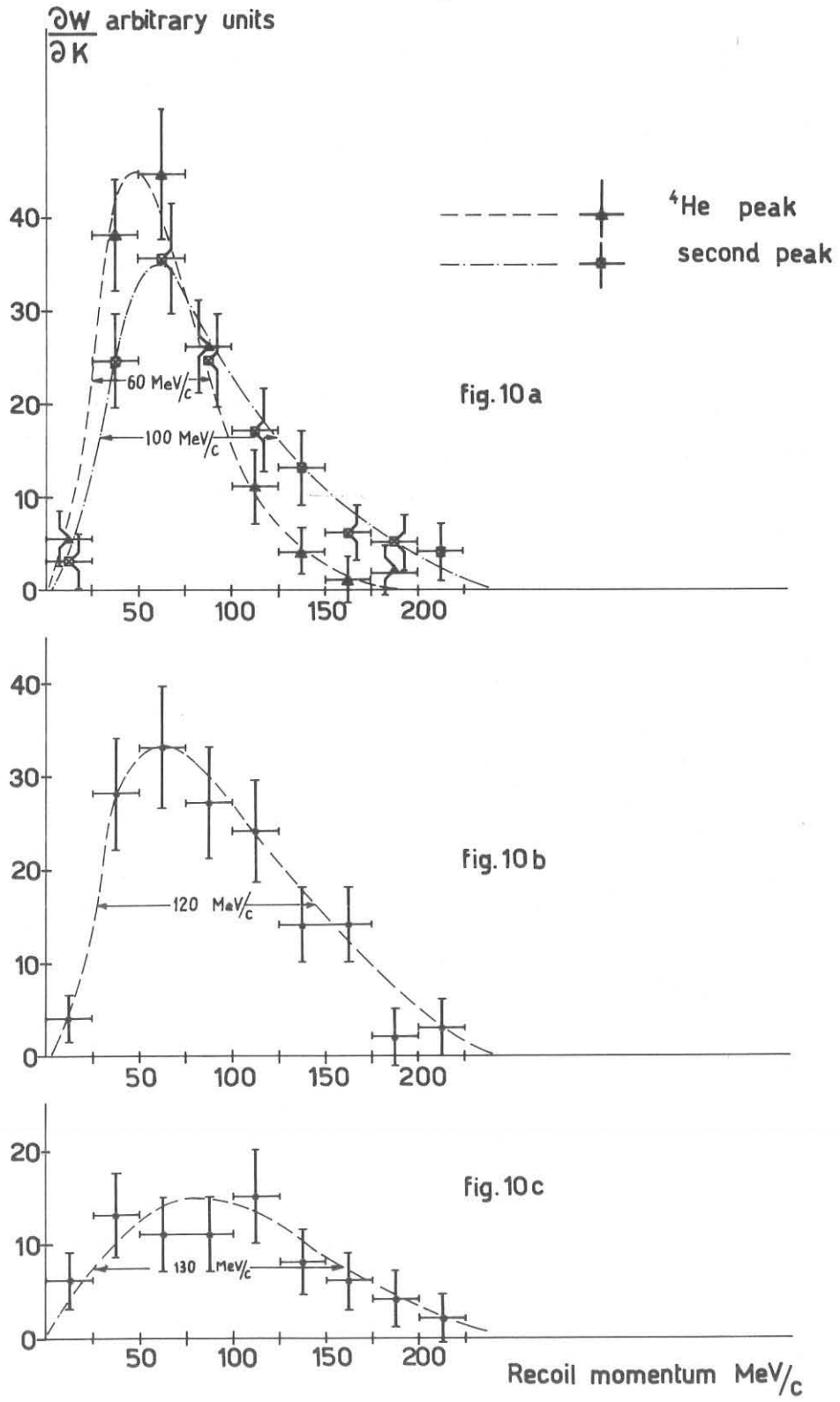
∂W/∂K arbitrary units
4He peak
second peak
60 MeV/c
100 MeV/c
fig.10a
120 MeV/c
fig.10b
130 MeV/c
fig.10c
Recoil momentum MeV/c

Fig.11

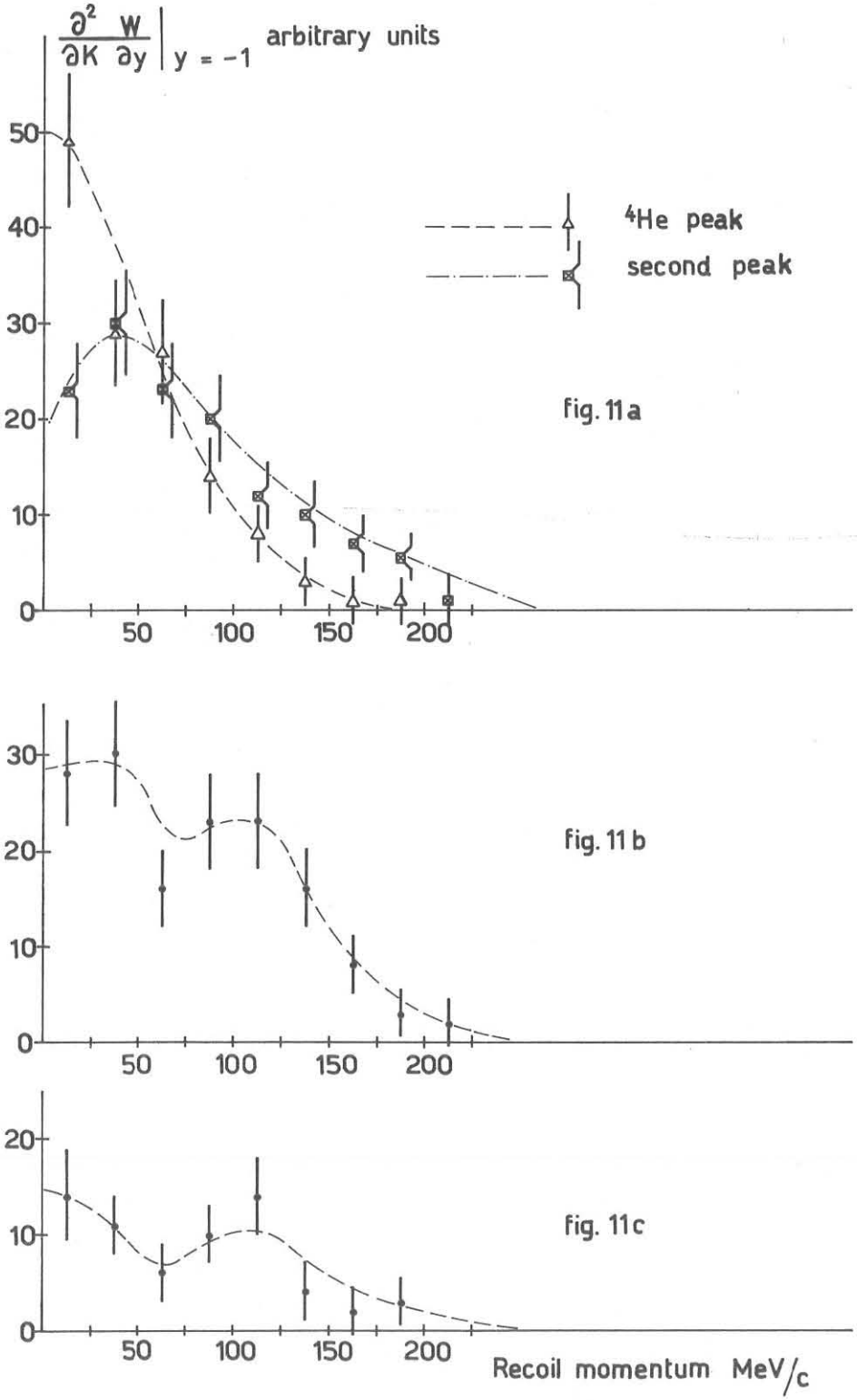
$\frac{\partial^2 W}{\partial K\ \partial y}\Big|_{y=-1}$ arbitrary units
50
40
30
20
10
0
50
100
150
200
^{4}He peak
second peak
fig. 11a
30
20
10
0
50
100
150
200
fig. 11b
20
10
0
50
100
150
200
fig. 11c
Recoil momentum MeV/c